ORIGINAL PAPER



Modal energy exchanges in an impulsively loaded beam with a geometrically nonlinear boundary condition: computation and experiment

Alireza Mojahed : Yang Liu · Lawrence A. Bergman · Alexander F. Vakakis

Received: 10 March 2020/Accepted: 11 December 2020/Published online: 3 January 2021 © The Author(s), under exclusive licence to Springer Nature B.V. part of Springer Nature 2021

Abstract The capability of a geometrically nonlinear boundary condition, i.e., a strong local nonlinearity, in "redistributing" a broadband input energy (generated by an impulsive load) among the vibration modes of a cantilever Euler-Bernoulli beam is investigated. It is shown that this modal energy redistribution increases the inherent capacity of the cantilever for passive energy dissipation. The nonlinear boundary condition is realized by grounding the free end of the cantilever through an inclined linear springdamper pair with initial angle of inclination ϕ_0 relative to the neutral axis of the beam while at rest. For $\phi_0 < 90^\circ$, the inclined spring-damper pair is geometrically nonlinear, whereas in the limiting case $\phi_0 = 90^{\circ}$ the boundary condition becomes *linear*. To study the nonlinear modal energy redistribution in the cantilever, a multi-step system identification method to identify the unknown parameters of the experimental fixture is employed; this informs a computational

A. Mojahed (⋈) · A. F. Vakakis Department of Mechanical Science and Engineering, University of Illinois, Urbana, IL, USA e-mail: mojahed2@illinois.edu

Y. Liu

State Key Laboratory of Mechanics and Control of Mechanical Structures, Nanjing University of Aeronautics and Astronautics, Nanjing, China

L. A. Bergman Department of Aerospace Engineering, University of Illinois, Urbana, IL, USA

reduced-order finite element (FE) model of the fixture. First, the Multi-input Multi-output Frequency Domain Identification (MFDID) technique to analyze the experimental frequency response functions of the "base" linear cantilever without the boundary condition is employed and its modal parameters are identified. Next, the boundary condition for the limiting angle $\phi_0 = 90^{\circ}$ is imposed, so that again a linear fixture is obtained. Through reconciliation of computational and experimental measurements, the (linear) stiffness and damping coefficients of the boundary are identified, as well. Finally, by varying the angle of inclination in the range $0^{\circ} \le \phi_0 < 90^{\circ}$, the nonlinear transient responses of the identified FE model with the nonlinear boundary condition are computed and projected onto the linearized modal basis of the system in the limit of zero energy. The computational FE results favorably compare with experimental measurements. Following this, the timeaveraged modal energies of the system are computed and used to estimate the portion of the total energy of the beam allocated to each mode. Additionally, by employing these modal energies one may study and track the nonlinear energy exchanges between subsets of modes for different angles of initial inclination ϕ_0 of the nonlinear boundary attachment. The computational results are validated by experimental measurements, thus highlighting the predictive capacity of the computational FE model. In the last step, a scalar measure for modal energy exchange is defined by



computing the maximum fluctuation in the percentage of each of the instantaneous modal energies that is the maximum percentage of energy being exchanged by the modes. This measure proves to be dependent on both the initial energy and the initial angle of inclination ϕ_0 . Again, experimental measurements favorably compare to computational FE simulations.

Keywords System identification · Cantilever beam · Geometrically nonlinear boundary condition · Modal energy exchange · Hardening, softening nonlinearity

1 Introduction

The presence of local strong nonlinearities in structures can greatly affect their dynamics. Indeed, in a series of works intentionally induced local nonlinearities have been exploited through implementation of targeted energy transfer (TET) in diverse systems with different types of nonlinearity [1–20]. Geometric nonlinearity is one type that can be achieved conveniently by arranging appropriately the configurations of stiffness-damper attachments. Due to their simplicity in realization and building, geometrically nonlinear elements have been widely used, especially in vibration mitigation systems [12, 14, 21–23]. For instance, Moore et al. [15] showed that two stores attached through geometrically nonlinear elements to the wings of an otherwise linear model airplane drastically affect its global dynamics under broadband excitation, resulting in more efficient dissipation of energy. In another application, a quasi-zero-stiffness passive nonlinear vibration isolator was studied [21]; the proposed vibration isolator could exhibit negative stiffness depending on the geometric parameters of the system, thus introducing softening nonlinear characteristics to the system. Also, Sarlis et al. designed and experimentally tested a geometrically nonlinear vibration isolation system with the capacity to exhibit softening stiffness characteristics due to geometric effects in order to protect structures from seismic loads [23]. More recently, Liu et al. [12] employed a similar geometrically nonlinear element as that studied in [22] to create a nonlinear vibration absorber, i.e., a nonlinear energy sink (NES), for a primary linear single degree-of-freedom (SDOF) oscillator under harmonic excitation. Through analytical

computational studies, they proved that by tuning the geometric parameter of the nonlinearity, unwanted high amplitude branches of the frequency responses could be eliminated. Mojahed et al. [24] also showed that the same geometric nonlinearity as in [12, 22] can be used very effectively for vibration isolation of systems under broadband excitation. They showed that this specific nonlinearity is capable of scattering energy from low to high frequencies, thereby reducing the displacements or strains that the main structure experiences, resulting in a lower likelihood of failure.

In practical problems where geometric effects are employed to achieve nonlinear behaviors, geometrically nonlinear damping is also, inevitably, present and sometimes plays a significant role in the dynamics. In fact, perhaps surprisingly it has been shown that geometrically nonlinear damping effects can induce modal instabilities in nonlinear multi-degree-of-freedom systems [25]. Moreover, it has been analytically and experimentally shown that in impulsively loaded SDOF systems geometrically nonlinear damping effects can slow down the transient dynamics [22]. We note at this point that another important type of geometrically nonlinear damping arises from large deformations or curvatures of continuous media such as beams, plates, and shells, where experimental and computational studies demonstrated that nonlinear dissipative effects can significantly influence the system behavior, especially at or near resonances [26–28]. Hence, accounting for geometrically induced nonlinear dissipative effects is important, especially in engineering systems composed of flexible parts.

In this work, the efficacy of a local nonlinearity in the form of a geometrically nonlinear boundary condition to "redistribute" impulsive energy in the modal space of a linear cantilever Euler–Bernoulli beam is investigated. Indeed, it is shown that such a local nonlinear boundary effect allows for intense nonlinear energy scattering in the frequency domain, yielding faster energy dissipation by the inherent damping capacity of the structure itself.

In particular, the nonlinear boundary condition is realized by grounding the free end of the cantilever beam through an inclined *linear* spring-damper pair with an initial angle of inclination ϕ_0 relative to the neutral axis of the beam while at rest. For $\phi_0 < 90^\circ$ the inclined spring-damper pair is *geometrically nonlinear*, whereas in the limiting case of $\phi_0 = 90^\circ$ the



boundary condition becomes *linear*. The system configuration is similar to the geometric nonlinearity studied in [12, 22, 24].

In the first section of this work, the experimental fixture and its associated reduced-order finite element (FE) model are introduced. Next, a two-step system identification technique is employed and the FE model is updated to reproduce the response of the experimental fixture. The system identification technique aims for accurate estimation of the system parameters of the cantilever and the inclined spring—damper pair of the boundary condition and consists of the following steps:

- (i) Implementation of the Multi-input Multi-output Frequency Domain Identification (MFDID) technique [29] to analyze the frequency response functions of the "base" linear cantilever beam, i.e., the cantilever without the boundary condition, subject to an impulsive load. This yields the modal parameters of the base cantilever, i.e., the natural frequencies and modal damping ratios.
- (ii) The results of the previous step inform the FE model of the base cantilever. To identify the linear parameters of the inclined springdamper pair comprising the geometrically nonlinear boundary condition, the *linear* cantilever with the boundary condition at an initial angle of inclination of $\phi_0 = 90^\circ$ is considered. Employing time series reconciliation, i.e., matching the computational response of the FE model with experimental measurements, the stiffness and damping coefficients of the boundary condition are identified.

In the second section, the theoretical framework that enables studying of the nonlinear energy exchanges among the vibration modes of the beam induced by the geometrically nonlinear boundary condition is introduced. Applying this framework to both the results obtained from computation (by using the identified FE model) and experiment (by testing the experimental fixture), the modal energy flows in the system and the impulsive energy redistribution in the linear modal space of the cantilever are tracked. To quantify these energy exchanges by a scalar estimator, a measure to quantify their maximum values for different excitation levels and angles of initial

inclination, ϕ_0 , is defined. Through this measure, it is shown that not only does the excitation intensity play an important role in the amount of energy exchanged among the modes, but also that the modal energy exchange can be maximized by varying the angle ϕ_0 , hence increasing the capacity of the system to dissipate energy faster through its high frequency modes.

2 Experimental fixture and finite element (FE) model

Figure 1a depicts the fully instrumented experimental fixture consisting of the linear cantilever steel beam (Young's modulus 192 GPa, density 7784 kg/m³, cross-sectional area $8 \times 44.6 \text{ mm}^2$, length 1.76 m) with the geometrically nonlinear boundary condition composed of the inclined spring-damper pair at its left end. A closeup of the geometrically nonlinear boundary condition is presented in Fig. 1b; this particular boundary condition was studied in a previous work [22] and is achieved by grounding the free end of the cantilever through a 1/4 inch diameter steel rod whose bending stiffness and inherent damping provide the geometrically nonlinear compliance and dissipation during the transient motion of the system. In Fig. 1a, b the initial angle of inclination is $\phi_0 = 0^\circ$, but this angle can be varied by adjusting the position of the base of the steel rod through orthogonal slots. Figure 1c illustrates the corresponding computational model, which is composed of a linear FE model of the cantilever beam connected to ground by an inclined massless parallel pair of a linear spring and a linear viscous damper. We note that although the constituent parts of the boundary have linear constitutive laws, the overall boundary effect is strongly nonlinear due to the geometry and kinematics during the transient dynamics. The cantilever beam is instrumented by an array of 10 PCB accelerometers (models U356A11 and Y353B17) all with a nominal sensitivity of 1.02 mV/ (m/s²), distributed evenly along the length of the beam. The impulsive excitations are applied at the tip of the cantilever where the nonlinearity is attached, by a PCB model hammer (model 086D29) with a compliant rubber tip.

The FE model associated with the experimental fixture (Fig. 1c) consists of 10 Euler–Bernoulli linear



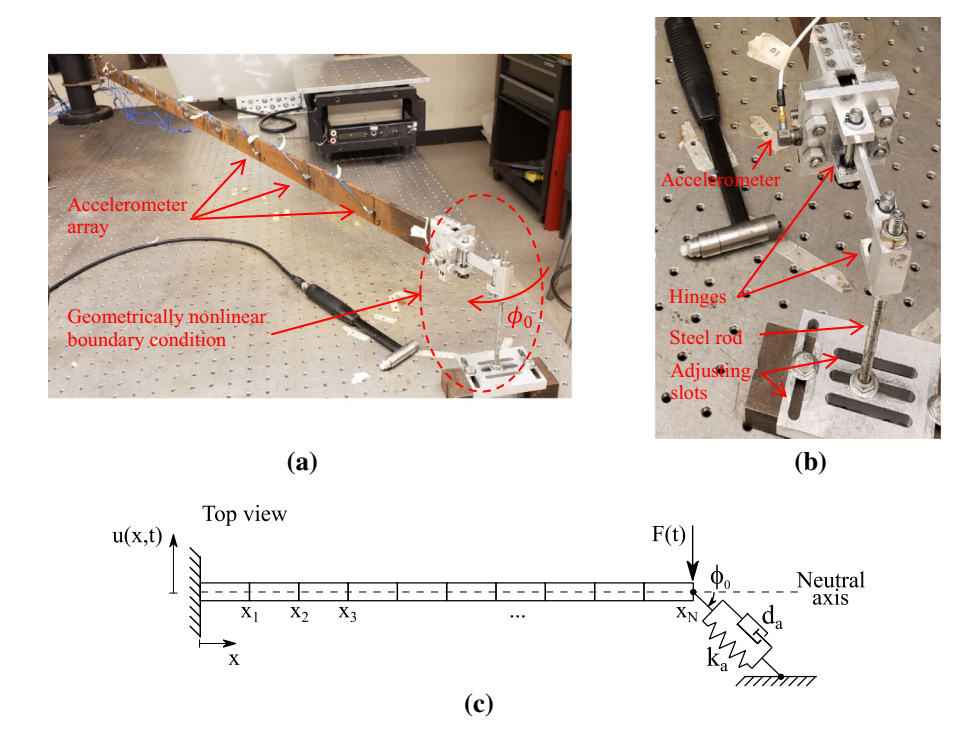


Fig. 1 Linear cantilever beam with geometrically nonlinear boundary condition: **a** experimental fixture instrumented with an array of accelerometers and **b** detail of the nonlinear boundary condition in the form of an inclined spring–damper

pair with $\phi_0=0^\circ$ (side view shown); **c** corresponding reduced-order FE model with boundary attachment with initial angle of inclination $0 \le \phi_0 \le 90^\circ$ (top view shown)

beam elements (N = 10) with the last node of the last element being grounded by means of an inclined spring–dashpot parallel pair. Assuming that only forces are applied to the beam (i.e., there are no applied moments), the Guyan reduction technique [30] is applied to the FE model, resulting in the following reduced-order computational model,

$$\begin{aligned} \mathbf{M}\ddot{\mathbf{u}} + \mathbf{C}\dot{\mathbf{u}} + \mathbf{K}\mathbf{u} + \mathbf{f}_{nl} &= \mathbf{F}(t), \\ \mathbf{u}(0) &= 0, \dot{\mathbf{u}}(0) &= 0, \end{aligned} \tag{1}$$

where overdot represents differentiation with respect to time, $\mathbf{u} = [u_1, u_2, \dots, u_{10}]^{\mathrm{T}}$ is the (10×1) nodal displacement vector at positions x_i along the cantilever (cf. Fig. 1c), and $\mathbf{M} = [m_{ij}]$ and $\mathbf{K} = [k_{ij}]$ are the (10×10) reduced mass and stiffness matrices of the FE model of the beam, and \mathbf{C} is the corresponding damping matrix. The non-homogeneous term $\mathbf{F}(t)$ is the (10×1) impulsive forcing vector; throughout this work, it was assumed that a single impulsive excitation is applied to the tip of the cantilever, which means that all the entries in $\mathbf{F}(t)$ are zero, except for the 10th that equals the applied impulse F(t). Explicit

expressions for the matrices M, and K have been reported in previous works [22, 31], whereas the damping matrix, C, is estimated by the system identification method of the next section.

Moreover, the (10×1) vector \mathbf{f}_{nl} in (1) incorporates the nonlinear forces applied to the cantilever by the geometrically nonlinear boundary condition whose elements, except the 10th, are zero. The 10th element, denoted by f_b , is expressed as [22]

$$f_b(u_{10};\phi_0) = d_a \left[\frac{(u_{10} + l_0 \sin \phi_0)^2}{(l_0 \cos \phi_0)^2 + (u_{10} + l_0 \sin \phi_0)^2} \right] \dot{u}_{10} + k_a (u_{10} + l_0 \sin \phi_0) \left[1 - \frac{l_0}{\sqrt{(l_0 \cos \phi_0)^2 + (u_{10} + l_0 \sin \phi_0)^2}} \right],$$
(2)

where l_0 is the natural length of the inclined spring—damper pair, d_a and k_a are its (linear) damping and stiffness coefficients, and ϕ_0 is the initial angle of inclination which is treated as an important geometric



system parameter. Similar to the damping matrix C, the coefficients k_a and d_a are estimated through system identification. It should be noted that the relation (2) includes both nonlinear stiffness and damping terms, and, depending on ϕ_0 and the oscillation amplitude, has been shown [22, 24] to possess complex nonlinear features such as, softening, hardening, and bi-stability.

2.1 System identification

The unknown parameters of the model (1) are estimated by a multi-step system identification study. In the first step, the nonlinear attachment is removed from the cantilever (obtaining the "base" linear cantilever), and then, the damping matrix C is identified by applying the Multi-input Multi-output Frequency Domain Identification (MFDID) method [29] to the frequency response functions of the beam. In the second step, the boundary attachment at the special angle of initial inclination $\phi_0 = 90^{\circ}$ is considered, in which case the system is again linear. Then, by applying time series reconciliation of the responses obtained by the FE model and the experimentally measured ones, the stiffness and damping parameters of the boundary attachment are identified. This process provides an estimation of all the unknown system parameters in the model (1).

2.1.1 Step 1: System identification of the modal damping of the base cantilever beam

Decoupling the boundary attachment from the cantilever the following linear "base" cantilever is obtained:

$$\mathbf{M}\ddot{\mathbf{u}} + \mathbf{C}\dot{\mathbf{u}} + \mathbf{K}\mathbf{u} = \mathbf{F}(\mathbf{t}),$$

$$\mathbf{u}(0) = 0, \dot{\mathbf{u}}(0) = 0.$$
 (3)

The MFDID method performs system identification in the frequency domain by analyzing frequency response (or transfer) functions. The MFDID technique was applied to the averaged direct receptance frequency response function (FRF) having as input the impulsive excitation applied to the tip of the base cantilever and as output the corresponding displacement at the same point; averaging was performed based on 16 different measured direct receptance FRFs in order to eliminate the effects of noise at low amplitudes. After identifying all the system

parameters of the base cantilever, the modal parameters predicted by the FE model were compared to the ones obtained by the experimental modal analysis.

Table 1 shows the comparison between the experimentally identified three lower natural frequencies of the base cantilever and those obtained by the FE model; in the same Table, the experimentally identified modal damping ratios for the same modes are also listed.

Figure 2 illustrates the comparison between the computationally reconstructed direct receptance FRF of the base cantilever and the experimentally measured one which highlights the predictive capacity of the FE model. It should be noted that the experimental FRF depicted in Fig. 2 was one of the 16 such measured FRFs that were used to compute the averaged direct receptance FRF used in the MFDID method (note the effects of noise at lower frequencies). Satisfactory agreement between computation and experiment is observed. This completes the first stage of the system identification process, after which the system parameters of the boundary attachment will be identified.

2.1.2 Step 2: System identification of the linear parameters of the boundary attachment

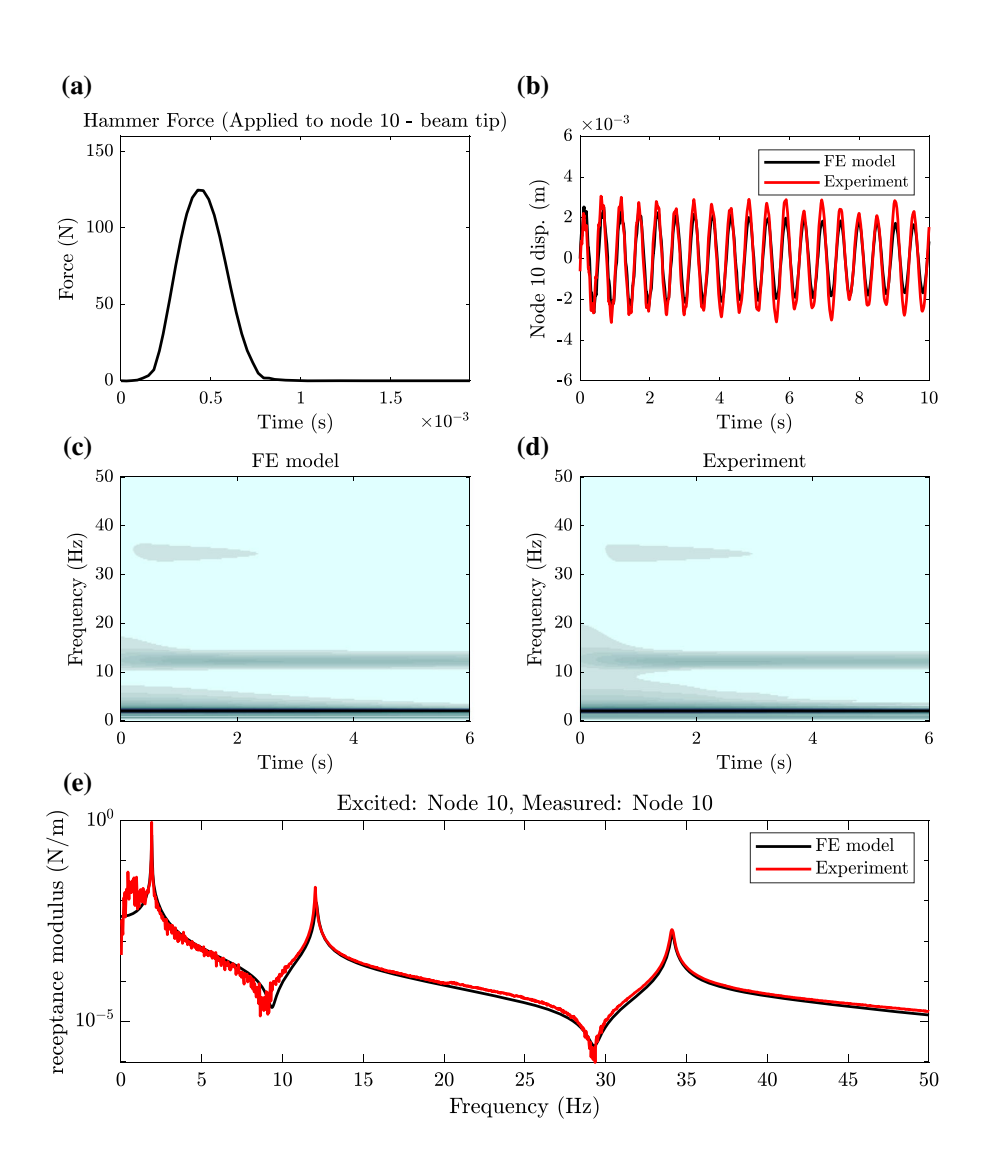
To identify the parameters associated with the boundary attachment, the spring-damper boundary attachment was configured to the special initial inclination angle $\phi_0 = 90^{\circ}$ yielding a *linear* system—cf. Figure 3. The system is then excited by an impulsive excitation at the beam tip using a modal hammer, and the beam response was recorded at the same point; this process was repeated for seven different excitations of varying intensities (cf. Table 2). For each forcing case, the temporal dependence of the applied impulses was experimentally measured; these measured impulses were then fed to the computational FE model during the reconciliation exercise described next.

In the last step of the identification procedure, the parameters of the (linear) spring-damper pair of the inclined boundary are estimated by performing direct time series reconciliation of the response of the FE model (with varying the two unknown parameters, k_a and d_a) and the experimentally measured response of the tip of the beam, subject to each of the seven applied impulsive excitations. To assess the success of the



Mode No.	Modal damping ratio	Experiment natural frequency (Hz)	FE model natural frequency (Hz)	Natural frequency relative error (%)
1	0.00226	1.90	1.91	0.5
2	0.00253	12.03	12.09	0.5
3	0.00151	34.08	34.12	0.1

Fig. 2 Comparison between computational response reconstruction and experimental measurement for the base cantilever: a impulsive force applied at the cantilever tip; b transient tip response, c and d wavelet transform spectra of the tip responses of the FE model and experimental fixture, respectively; and e computational and experimental direct receptance FRFs (red lines denote experimental measurements and black lines computational reconstructions). (Color figure online)



time series reconciliation the objective function, $S=1-R^2$, where R^2 is the coefficient of determination was considered. The average values for k_a and d_a computed from the corresponding values obtained from the beam tip response reconciliation for each excitation case are listed in Table 2.

A typical example of the reconciliation process is presented in Fig. 4, where the computationally reconstructed cantilever tip response (for the identified system parameters k_a and d_a) is compared to the experimentally measured one. This particular result corresponds to one of the seven applied impulsive



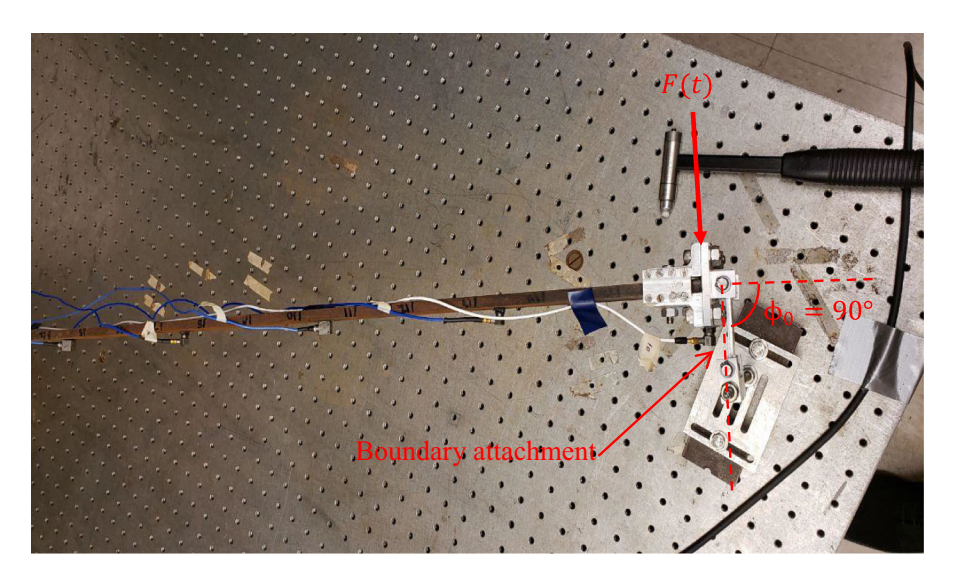


Fig. 3 Linear system configuration for initial angle of inclination $\phi_0 = 90^{\circ}$ of the boundary attachment for the second stage of the system identification (top view shown)

Table 2 Identified linear stiffness and damping coefficients of the boundary attachment

The bold values correspond to the averaged values of stiffness and damping we used in the computational model

Test No.	Max. force (N)	k_a (N/m)	d_a (Ns/m)	R^2
1	363.25	11,567.5	31.10	0.83
2	376.82	11,592.0	30.90	0.85
3	405.40	11,935.7	28.25	0.84
4	431.89	11,846.0	27.55	0.84
5	446.74	11,720.0	29.75	0.76
6	481.21	11,770.0	27.59	0.77
7	543.09	12,040.0	26.68	0.73
Average values		11,781.6	28.83	

excitation cases (cf. Table 2), and, in addition to time series comparison—cf. Figure 4a—a comparison of the corresponding wavelet transform spectra is also shown—cf. Figure 4c and d. Similar results were obtained for the other cases of impulsive excitations. These results confirm the accuracy of the nonlinear system identification process and validate the identified system parameters of the experimental system. A synopsis of the system identification is given in Table 3 and enables the study and experimental validation of the fully identified nonlinear model presented in (1).

3 Transient response of the cantilever beam with nonlinear boundary condition

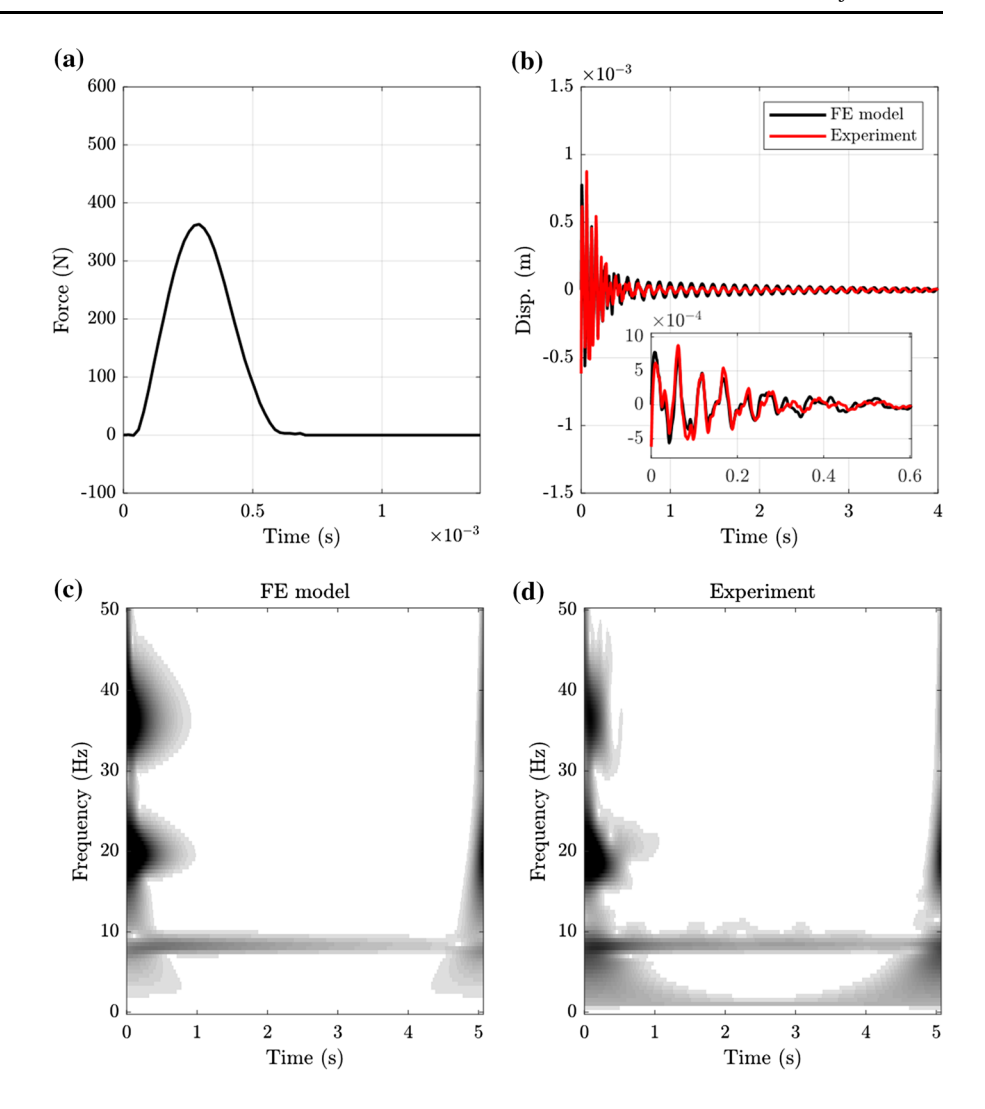
Considering the geometrically nonlinear boundary condition (2), it should be noticed that for $\phi_0 = 90^{\circ}$ the restoring force, f_b , degenerates to the following *linear* expression

$$f_b = d_a \dot{u}_{10} + k_a u_{10},\tag{4}$$

which contributes only linearly to the dynamics of the system. This, however, is not the case for an initial angle of inclination in the range $0 \le \phi_0 < 90^\circ$, where strongly nonlinear stiffness and damping effects are induced at the end boundary of the cantilever beam. In this section, the identified computational model for initial inclination angles less than 90° is validated, and certain aspects of the geometrically nonlinear



Fig. 4 Example of computational and experimental response reconciliation for the system with $\phi_0 = 90^\circ$ corresponding to one of the impulsive excitations of Table 2: a impulsive force applied to the tip of the beam; b response of the beam tip-insert shows the detail of early-time response (red line denotes experimental measurement, and black line computational FE reconstruction); and **c**, **d** wavelet transform spectra of the beam tip responses reconstructed by the FE model and measured in the experimental fixture, respectively. (Color figure online)



dynamics of this system are highlighted. For demonstration purposes, three systems corresponding to different values of ϕ_0 are considered in this section.

The case with $\phi_0=0^\circ$, which, as discussed below, yields a strongly nonlinear system is considered first. Indeed, this represents a special case for the dynamics since the nonlinear stiffness restoring force (2) exerted by the boundary is *non-linearizable*, i.e., it does not possess any linear component; this means that the linearized natural frequencies of the cantilever beam with the nonlinear boundary will be identical to those of the base cantilever beam (i.e., the beam with no nonlinear attachment at its end). Figure 5 depicts the displacement of the beam tip measured from the experiment and predicted by the FE model, in both the time and wavelet transform domains. For the specific

impulsive excitation considered (cf. Figure 5a), there is close agreement between the experimental and computational results, both in the initial high energy cycle and at later times (that is, after 2 s)—cf. Figure 5b. Moreover, the wavelet transform spectra of the two responses show great similarity, except for the $\sim 10 \text{ Hz}$ harmonic that appears in the experimental response but not in the computational one; this is the reason for the phase difference between the two responses in the interval 0.5 and 2 s—cf. Figure 5b. Moreover, due to the odd-symmetry with respect to the beam tip displacement of the restoring boundary force (2), the stiffness nonlinearity in this case is strictly hardening [22, 24]. This is evident in Fig. 5c and d where the frequency of the first mode—the shaded area in the 3-5 Hz range—decreases with time (or



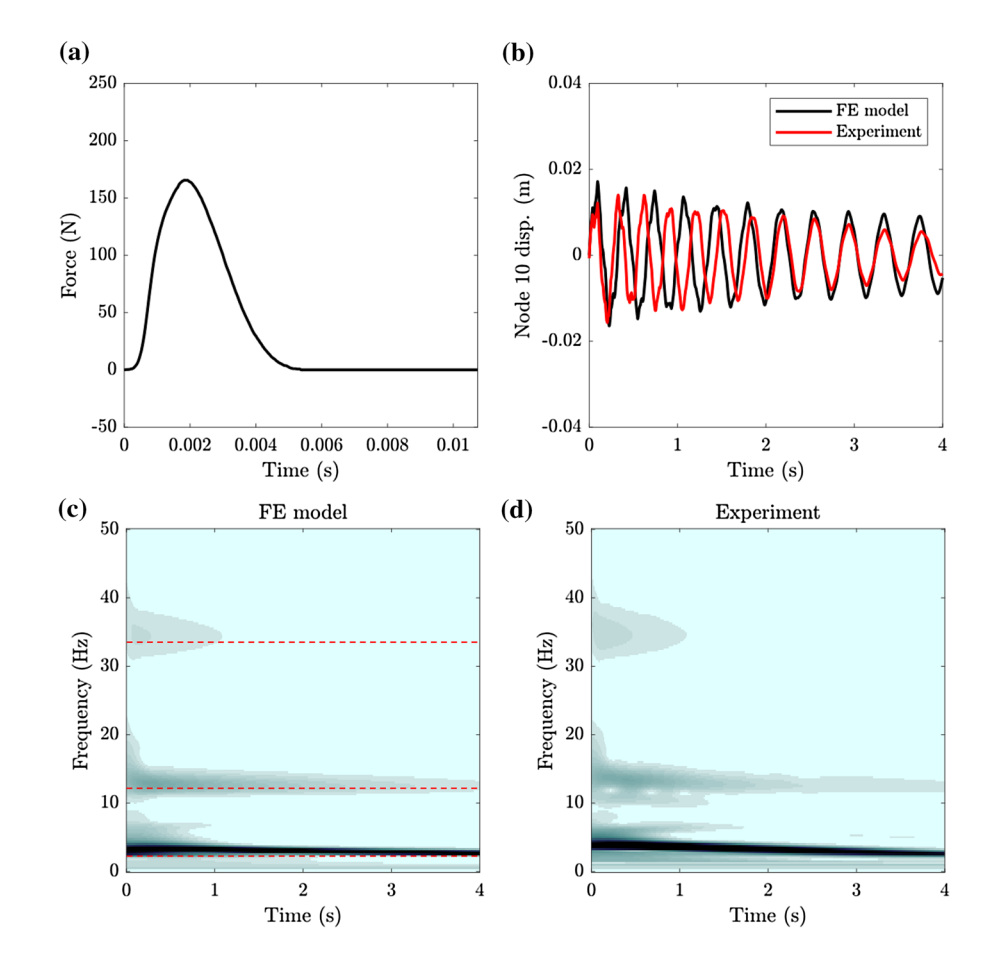
Table 3 Summary of the identified parameters of system (1)

Parameter	Value
Beam Length (m)	1.76
Young's Modulus (GPa)	192
Density (kg/m ²)	7784.0
Width (m)	0.0080
Height (m)	0.0446
Number of finite elements	10
Modal damping ratio—1st mode	0.0023
Modal damping ratio—2nd mode	0.0025
Modal damping ratio—3rd mode	0.0015
Added mass at the tip of the beam (kg)	0.21
k_a (N/m)	11,780.0
d_a (Ns/m)	28.83
l_0 (m)	0.05

equivalently, with energy). The dashed lines in Fig. 5c indicate the natural frequencies of the base cantilever, confirming that, indeed, the special initial inclination angle of $\phi_0=0^\circ$ does not introduce any linearized stiffness corrections in the dynamics of the system. Furthermore, comparing the nonlinear transient responses of Fig. 5 to those of the linear system with $\phi_0=90^\circ$, it is deduced that an overall softening of the transient dynamics (in the sense that it possesses lower linearized natural frequencies), as well as a reduced dissipative capacity (as the transient oscillations, undergoes slower decay—see also [22]).

Qualitatively different transient dynamics is realized when the initial angle of inclination is increased to $\phi_0 = 8^{\circ}$, with the corresponding results being presented in Fig. 6. Note that, similar to the case with $\phi_0 = 0^{\circ}$, the time series comparison between the two responses (cf. Fig. 6b) is in rather good agreement, as

Fig. 5 Comparison of the experimental and computational beam tip responses for $\phi_0=0^\circ$: a Impulsive force at the tip of the beam, \mathbf{b} time series (red line denotes experimental measurement and black line FE reconstruction), and c, d corresponding experimental and computational wavelet transform spectra, respectively; red dashed lines in (c) indicate the leading natural frequencies of the base cantilever-cf. Table 1. (Color figure online)





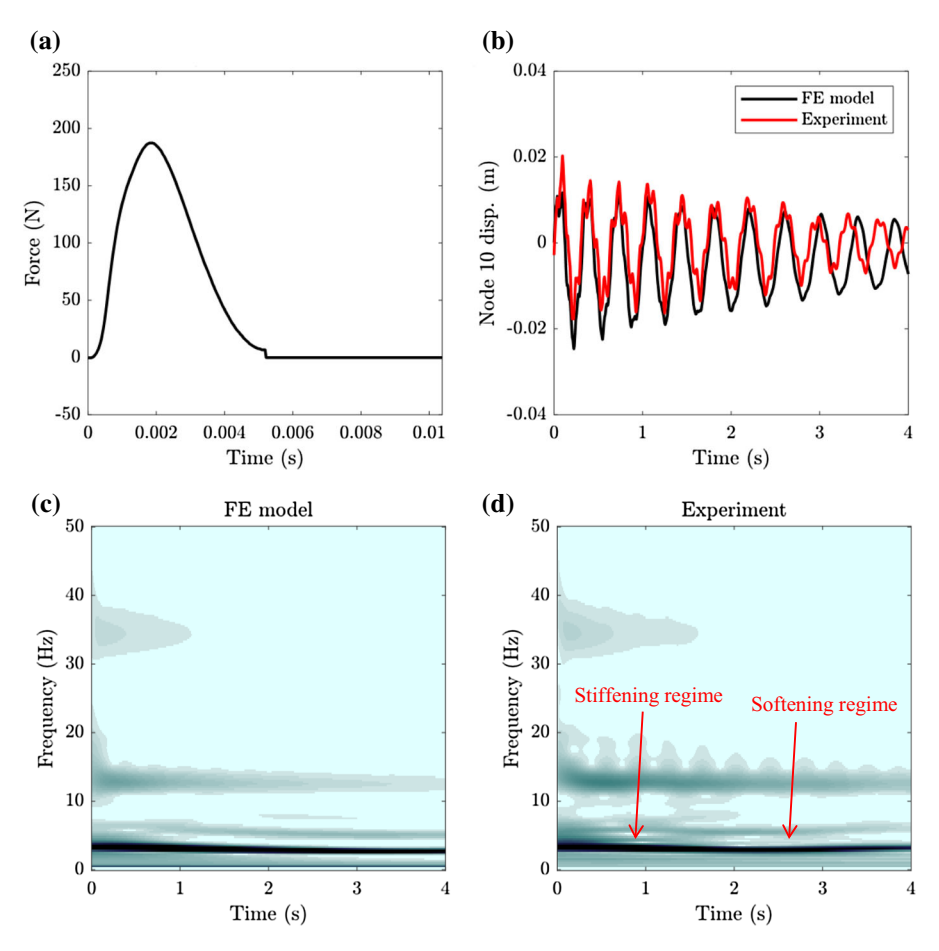


Fig. 6 Comparison of the experimental and computational beam tip responses for $\phi_0 = 8^\circ$: **a** impulsive force at the tip of the beam, **b** time series (red line denotes experimental

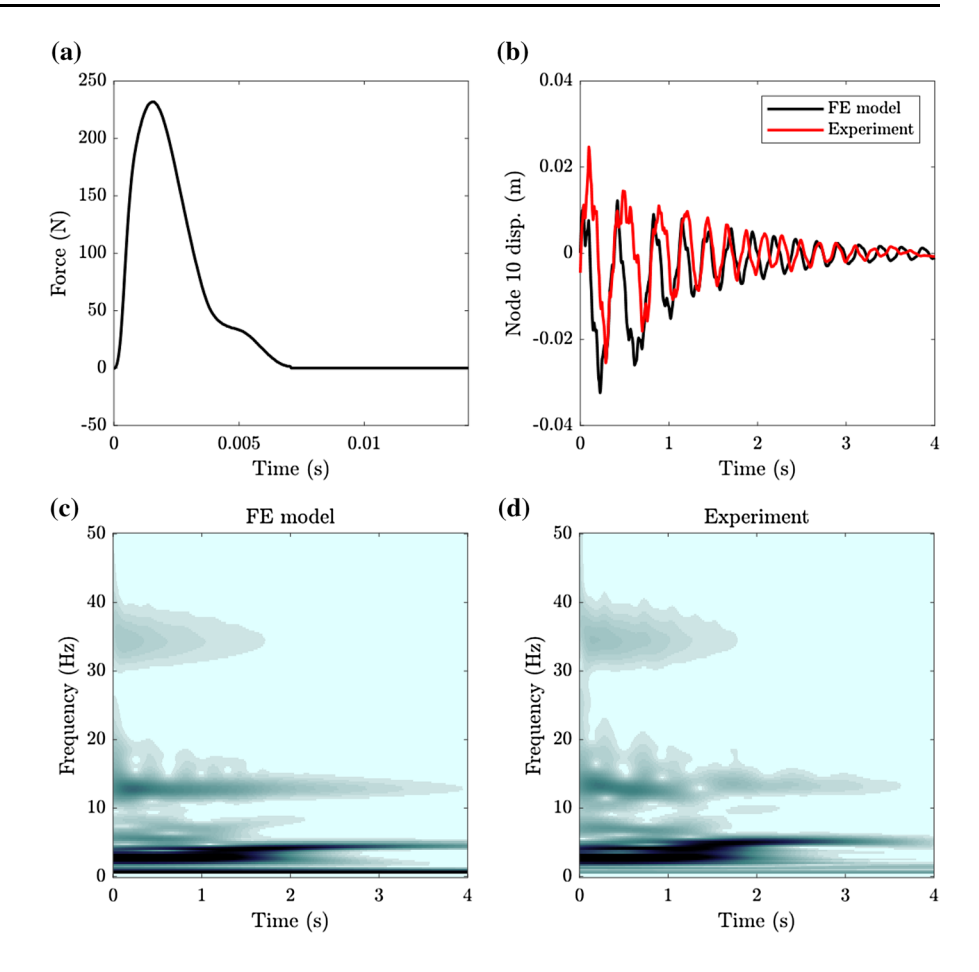
measurement and black line FE reconstruction), and \mathbf{c} , \mathbf{d} corresponding experimental and computational wavelet transform spectra, respectively

are the corresponding wavelet transforms spectra (cf. Fig. 6c, d). However, unlike the previous case where the response was purely hardening, in this case the restoring boundary force (2) is no longer oddsymmetric with respect to the beam tip displacement; as a result, the stiffness nonlinearity of the system cannot be characterized as being purely hardening. This result is reflected in the wavelet transform spectra, especially in the computational result depicted in Fig. 6d, where one can observe that the frequency of the lower mode of the beam initially decreases from 0 to 2 s—representing the stiffness hardening phase of the dynamics, before it starts increasing—representing the stiffness softening phase. This result, which is in agreement with an earlier work [22], indicates that for $\phi_0 = 8^{\circ}$ the dynamics is initially hardening in the highly energetic regime of the response and then softening in the later response regime at lower energy levels.

The stiffness softening phase of the transient dynamics becomes more pronounced as the initial angle of inclination, ϕ_0 , of the boundary attachment increases. This is demonstrated by the results depicted in Fig. 7 corresponding to $\phi_0=16^\circ$. Similar to the previous two cases, the computational and experimental responses are in good agreement, which validates further the FE model. Moreover, the wavelet transform spectra of Fig. 7c, d show *very prominent softening stiffness nonlinearities in the transient dynamics*; this is evident by the monotonic increase in the frequency of the lower mode with time, or, equivalently with decreasing energy. In addition, the early-time transient response is *more broadband*, indicating the enhancement of the nonlinear effects



Fig. 7 Comparison of the experimental and computational beam tip responses for $\phi_0=16^\circ$ a Impulsive force at the tip of the beam, b Time series (red line denotes experimental measurement and black line FE reconstruction), and c, d corresponding experimental and computational wavelet transform spectra, respectively



in this highly energetic regime of the dynamics. The broadband feature of the nonlinear transient response indicates the generation of harmonics in the response, which is to be expected in this system due to strong geometric nonlinearities. As discussed below, nonlinear harmonic generation may yield intense energy transfers between modes, in contrast to the linear base cantilever beam where modal interactions are not possible (as in any linear time invariant system). Next the nonlinear modal energy exchanges are studied in more detail.

As mentioned previously, a common feature in all three cases discussed earlier is the generation of harmonics due to the geometric nonlinearity of the boundary. These harmonics can lead to intense energy exchanges between their associated fundamental harmonic and other modes of the structure through resonance captures and internal resonances [3, 15, 20, 24]. To study such nonlinear energy exchanges, need to introduce we modal transformation for the system dynamics based on the vibration modes of the linearized Hamiltonian system (i.e., the system with no damping or external forcing terms). The basis for the modal transformation is obtained by solving an eigenvalue problem resulting from (1) and (2) by setting $\mathbf{C} = \mathbf{0}$, $\mathbf{F}(t) = \mathbf{0}$ and $d_a = 0$ and taking the limit $||\mathbf{u}|| \to 0$, where ||.|| denotes the L2 norm operator. This way, in the low energy limit one is able to define the base formed by the linearized modes of the cantilever beam—boundary attachment system in the limit of small response amplitudes when the geometrically nonlinear effects are nearly negligible. The derived linearized eigenvalue problem is then written as

$$\left[-\omega_i^2(\phi_0)\mathbf{M} + \bar{\mathbf{K}}(\phi_0)\right]\boldsymbol{\varphi_i}(\phi_0) = \mathbf{0},\tag{5}$$

where $\omega_i(\phi_0)$ and $\boldsymbol{\varphi_i}(\phi_0)$ are the i-th linear natural frequency and mass-orthonormalized mode shape of the system in the low energy limit, respectively, and $\mathbf{M} = \begin{bmatrix} m_{ij} \end{bmatrix}$ and $\bar{\mathbf{K}}(\phi_0) = \begin{bmatrix} \bar{k}_{ij}(\phi_0) \end{bmatrix}$ are the reduced



 (10×10) mass and linearized stiffness matrices, respectively, where

$$\bar{k_{ij}}(\phi_0) = \begin{cases} k_{i,j} & i, j = 1, 2, \dots, 9 \\ k_{(10)(10)} + k_a \sin^2 \phi_0 & i = j = 10. \end{cases}$$
 (6)

and the elements m_{ij} and k_{ij} are the mass and stiffness elements of the FE model of the cantilever beam (cf. discussion in Sect. 2). Moreover, the term $k_a \sin^2 \phi_0$ represents the effective linearized stiffness of the geometrically nonlinear boundary attachment in the low energy limit, i.e., $\lim_{u_{10}\to 0} \partial f_b(u_{10};\phi_0)/\partial u_{10} =$

 $k_a \sin^2 \phi_0$ [22, 24]. We emphasize at this point that both the linearized stiffness matrix, and linearized natural frequencies and mode shapes depend on the initial angle of inclination of the boundary attachment.

The linearized modal matrix $\Phi(\phi_0) = [\varphi_1(\phi_0)|\varphi_2(\phi_0)|\cdots|\varphi_{10}(\phi_0)]$ creates a linear modal basis on which the transient response the system can be projected as follows

$$\mathbf{\eta} = \mathbf{\Phi}^{-1}(\phi_0)\mathbf{u},\tag{7}$$

where $\mathbf{\eta} = [\eta_1, \eta_2, \eta_3, \dots, \eta_{10}]^T$ is the vector of modal displacements, containing the projected nonlinear nodal responses of the cantilever beam onto the linearized modal basis defined by the eigenvalue (5). It should be noted, however, that the linearized modal basis derived by (5) has physical meaning only in the low energy limit of the nonlinear dynamics and changes when the initial angle of inclination of the boundary attachment changes.

Once the linearized modal responses (7) are obtained, the associated averaged modal energies can be computed using the methods employed by [3, 15, 32] relying on the envelope of the time series of the kinetic energy of the system

$$\bar{E_i}(t) = \langle \frac{1}{2} \dot{\eta}_i^2 \rangle_t, \tag{8}$$

where \bar{E}_i , $i=1,2,\ldots,0$, is the averaged energy associated with the i-th linearized mode. Moreover, the operator \cdot_i denotes averaging with respect to time and is computation is accomplished by fitting a cubic spline to the local maxima of the corresponding kinetic energy [32]. Using relations (8), the i-th instantaneous effective modal damping ratio (EMDR) can be defined by [32]:



The instantaneous EMDRs (9) provide a valuable quantitative measure regarding the individual mode participation in the nonlinear modal interactions during the transient dynamics, especially when compared with the (nominal) inherent modal damping values listed in Table 1. Indeed, an instantaneous EMDR greater (smaller) than the nominal damping modal ratio indicates that that specific mode transfers energy to (receives energy from) other modes [3, 15, 32]; hence, these measures provide physical insight on the transient nonlinear energy exchanges between the beam modes, induced by the nonlinear boundary attachment. In the next section, we will apply the developed framework to experimental measurements and compare them with computational predictions.

4 Transient nonlinear modal interactions

In this section, we study the energy exchanges that occur among the first three nonlinear modes of the cantilever beam by employing relations (8) and (9). Since these modal energy exchanges depend solely on the geometric nonlinearity, the two most relevant parameters that can affect the intensity of the modal interactions are (i) the input energy, i.e., the intensity of the applied impulsive excitation, and (ii) the initial angle of inclination of the boundary attachment, ϕ_0 .

First, a low intensity impulsive excitation with $\phi_0 = 0^{\circ}$, cf. Fig. 5 is considered. In the following study, both experimentally measured responses along the cantilever (obtained through an array of 10 accelerometers-cf. Fig. 1a), as well as computational responses provided by the FE model; we will "project" these measured responses onto the linearized modal basis of the beam—attachment system obtained in the limit of small energies will be analyzed (note that this modal bases depends on the angle of inclination, so it is expected to change with varying ϕ_0). This enables computation of the associated averaged modal energies (8) and the EMDRs (9) for the three leading cantilever modes. In Figs. 8, 9, and 10, the modal responses with close agreement noted between the computational predictions and the experimental measurements are presented. Since these



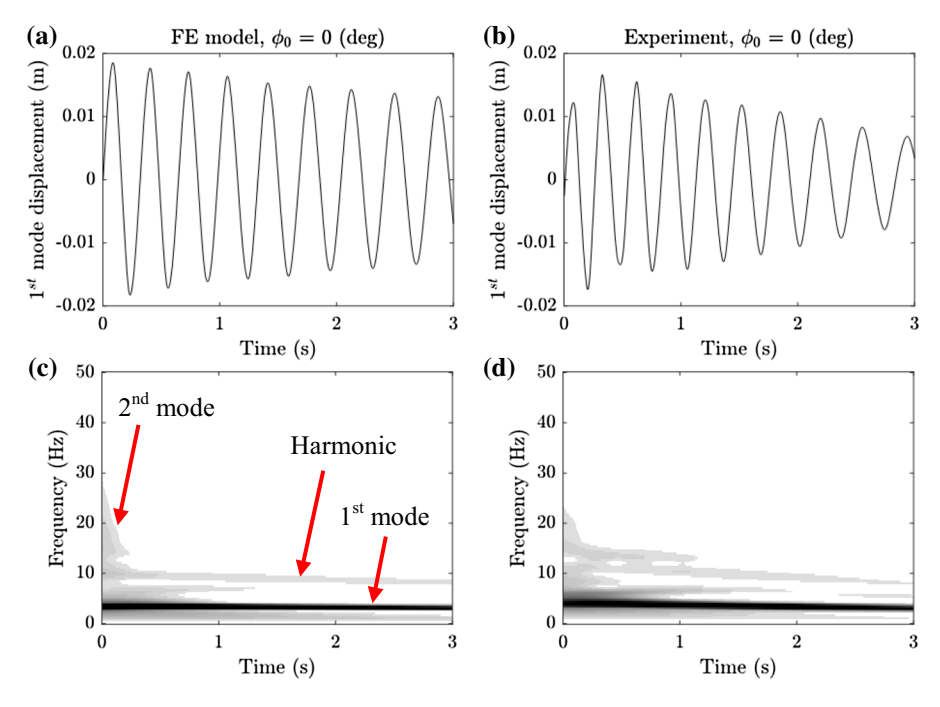


Fig. 8 Response of the first nonlinear mode for low impulse excitation and $\phi_0 = 0^{\circ}$ (cf. Fig. 5): **a**, **c** Computational prediction, and **b**, **d** experimental measurement

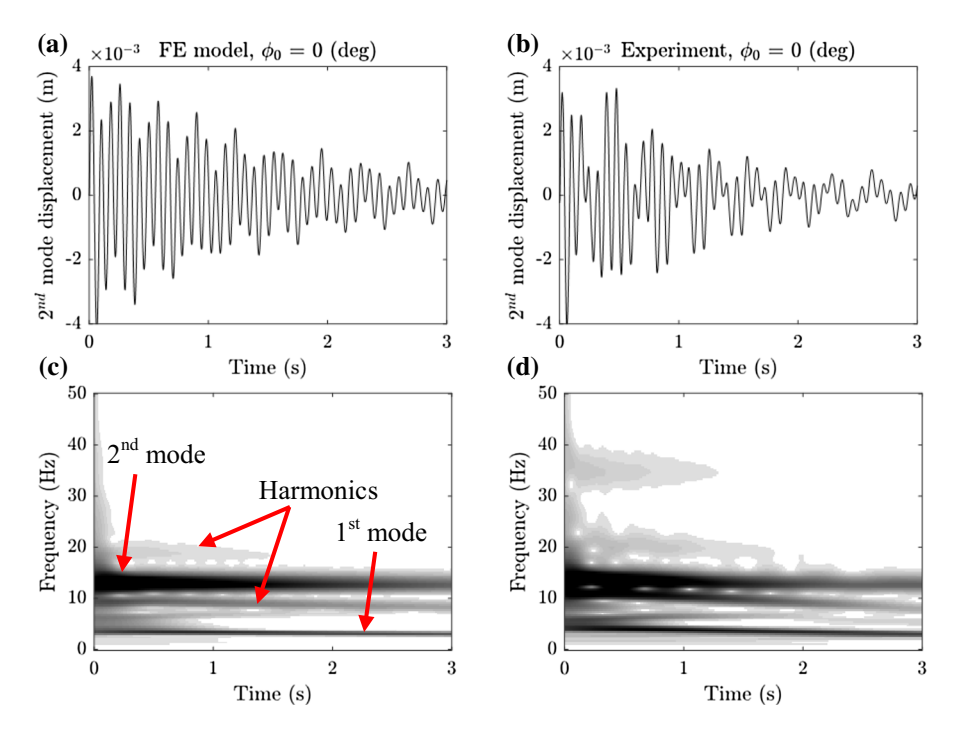


Fig. 9 Response of the second nonlinear mode for low impulse excitation and $\phi_0 = 0^{\circ}$ (cf. Fig. 5): **a**, **c** Computational prediction, and **b**, **d** experimental measurement



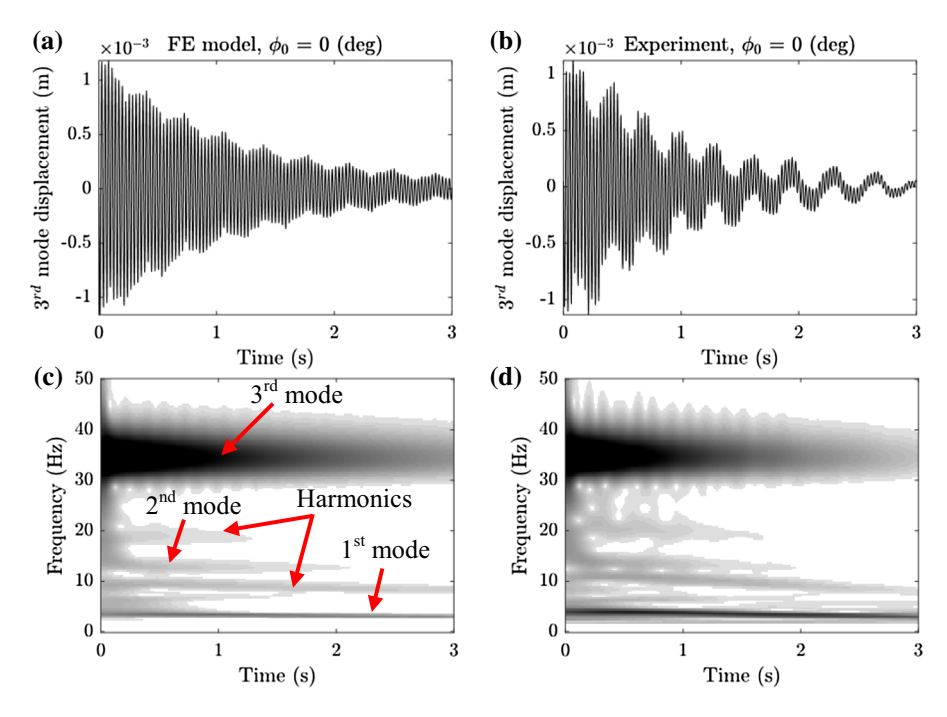


Fig. 10 Response of the third nonlinear mode for low impulse excitation and $\phi_0 = 0^{\circ}$ (cf. Fig. 5): **a**, **c** Computational prediction, and **b**, **d** experimental measurement. (Color figure online)

modes correspond to the geometrically nonlinear system, they will be referred to as "nonlinear modes" of the cantilever beam.

Considering the response of the lowest frequency nonlinear mode in Fig. 8, the dominant presence of the first nonlinear mode is observed, but also note the presence of its higher harmonics generated due to the geometric nonlinearity. Moreover, traces of the second nonlinear mode also appear in the wavelet transforms, which indicate possible interaction of the first and second nonlinear modes. This will later be verified by examining the averaged modal energies and modal damping ratios. Figure 9 depicts the second nonlinear modal response, and from the corresponding wavelet transforms not only the presence of the second nonlinear mode itself can be observed, but also the very pronounced presence of the first mode and its harmonics. Because of the presence of the first nonlinear mode, the second nonlinear mode is expected to exhibit strong and sustained modal interactions with the lower frequency first nonlinear mode. Similar observations can be made for the response of the third nonlinear mode, cf. Fig. 10. For this particular mode, not only the first mode and its harmonics are present, but also there are weak traces

of the second nonlinear mode. Such modal interactions (that are clearly observed in the corresponding wavelet transforms) are solely due to the local geometric nonlinearity at the boundary of the beam, since in the corresponding linear system (i.e., without the boundary) no modal interactions are possible.

Based on the experimental measurements and the computational results, the energy exchanges and interactions between the first three nonlinear modes of the cantilever can be determined by computing the corresponding averaged modal energies normalized by the instantaneous total energy of the system as follows

$$\hat{E_i}(t) = \frac{\bar{E_i}(t)}{E_{tot}(t)} \times 100,$$

$$E_{tot}(t) = \frac{1}{2} \mathbf{u}^{\mathrm{T}} \mathbf{M} \mathbf{u} + \frac{1}{2} \mathbf{u}^{\mathrm{T}} \mathbf{K} \mathbf{u} + E_{nl}$$
(10)

where E_{nl} is the instantaneous potential energy of the nonlinear boundary and is computed as:

$$E_{nl} = \frac{1}{2} k_a \left[\left(l_0^2 + 2l_0 u_{10} \sin \phi_0 + u_{10}^2 \right)^{1/2} - l_0 \right]^2.$$
 (11)



Then, the normalized effective damping ratios, ζ_i , for the first three nonlinear modes are computed directly from the EMDRs (9) according to the relation

$$\zeta_i = \frac{\bar{\zeta}_i(t)}{\lim_{t \to \infty} \bar{\zeta}_i(t)} \tag{12}$$

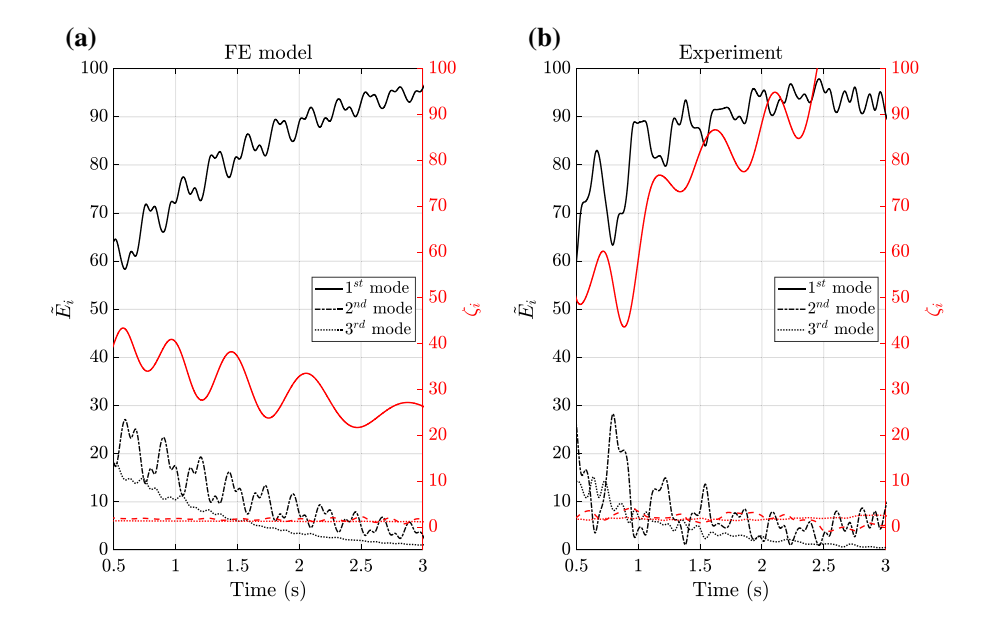
where, unlike the numerator that is computed both from experimental and computational results, the limiting value in the denominator is evaluated computationally, i.e., from the FE model (since evaluating it computationally is not possible due to the availability of only finite duration experimentally measured data).

Figure 11 depicts the normalized modal energies and effective damping ratios for the leading three modes, obtained from both the experimental measurements and the computational predictions. It should be noted that, due to numerical end effects caused by using either natural or clamped spline fitting in (8), the first and last 0.5 s of data has been neglected. Considering first the normalized modal energies in Fig. 11a and b, it should be noted that they fluctuate with time, meaning that the associated cantilever modes either lose (when the plots decrease) or gain (when the plots increase) energy as they nonlinearly interact with other modes. Moreover, as the energy of the first (lower frequency) nonlinear mode decreases, that of the second mode increases. This indicates that a portion of the energy that the first nonlinear mode is transferred to the second nonlinear mode; hence, the valleys (peaks) of the energy of the first mode are synchronized with the peaks (valleys) of the second mode, proving that these nonlinear modes consistently exchange energy between them in a nonlinear beat phenomenon. However, it is observed that with increasing time the transient dynamics of the system gradually becomes dominated by the first cantilever nonlinear mode; this is to be expected, since, being the mode with the lowest frequency, the first mode has smaller dissipative capacity compared to the higher frequency modes. Finally, the modal energies computed from the experimental measurements and the computational model show the same trend and agree both qualitatively and quantitatively; this demonstrates once more the predictive capacity of the computational model.

Examining then the instantaneous normalized dissipation rates, similar conclusions can be drawn. Indeed, the fluctuations in the instantaneous normalized modal damping ratios provide a clear picture as to when the corresponding cantilever modes receive or shed energy, depending on whether their values decrease or increase, respectively. Moreover, Fig. 11a and b implies a qualitative difference between the computational and experimental normalized damping ratios for the first mode, in the sense that whereas it exhibits a decreasing trend in the computational result (cf. Fig. 11a), this changes to an increasing trend for the experimental measurement (cf. Fig. 11b). The

Fig. 11 Case of low impulse excitation and $\phi_0 = 0^\circ$ (cf. Fig. 5): Instantaneous normalized modal energies (10) (black curves—left axes) and instantaneous normalized damping ratios (12) (red curves—right axes) for the three leading cantilever modes, a Computational predictions and b experimental

measurements.1





conjecture is that the increase in the experimental result is due to the presence of Coulomb friction at the joint coupling the nonlinear attachment to the beam—cf. Fig. 1c; such nonlinear dissipative effects are not taken into account in computational model where all dissipative elements are assumed to be linear and viscous. Regarding the normalized damping ratios for the second and third cantilever modes, these are small and exhibit small fluctuations.

In attempt to establish a single scalar measure that quantifies the maximum modal energy exchange for each nonlinear mode, the difference between each local maximum and its adjacent minimum for each normalized instantaneous modal energy is computed and the maximum value of such difference, $\Delta \hat{E_i}$, is recorded. For the considered case of impulsive excitation and nonlinear boundary, we computed these maximum energy exchange measures as $\Delta \hat{E}_1^c =$ -7.13% and $\Delta \hat{E}_2^c = 5.88\%$ from the computational results, and $\Delta\hat{E}_1^E = -17.12\%$ and $\Delta\hat{E}_2^E = 10.86\%$ from the experimental measurements; note that negative values correspond to decreasing energy, while positive values correspond to increasing energy. Hence, both the computational and experimental results show that there is nonlinear low-to-high frequency transfer of energy from the first to the second mode, although the computational model appears to underestimate the intensity of the energy exchange.

As a second case, the system with $\phi_0 = 16^{\circ}$ subject to high intensity impulsive excitation is considered cf. Fig. 7. Following the modal projection scheme discussed previously, i.e., relations (5)–(7), the experimentally measured and computationally predicted responses of the sensing locations along the cantilever are projected on to the linearized modal basis obtained in the low energy-limit. This yields a set of transient modal responses, as expressed previously. The plots depicted in Fig. 12 depict the first modal response in the temporal and frequency domains. It should be noted that even though the transient dynamics is strongly nonlinear, not only the computational and experimental time series show good agreement, but also their corresponding wavelet transform spectra agree as well. Up to 0.5 s, both wavelet transforms show hardening nonlinear behavior (signified by the fact that the instantaneous frequency of the mode decreases with increasing time—or decreasing energy). After that initial hardening phase, however, the frequency of the first mode along with its harmonics increases with time, representing the softening phase of the nonlinear dynamics. Comparing the computational and experimental wavelet transform spectra of Fig. 12 with those of Fig. 8, it is noted that, by increasing the initial angle of inclination from $\phi_0 =$ 0° to $\phi_0 = 16^{\circ}$, the number and intensity of the higher harmonics are increased, and these strongly affect the transient dynamics. In particular, unlike the case of $\phi_0 = 0^\circ$ where only one harmonic is present in the first mode response, in the present case there are three distinct harmonics that appear over extended periods of time. This highlights the enhanced broadband nature of the nonlinear response for this increased initial angle of inclination.

Due to the presence of the higher number of intense harmonics for this value of ϕ_0 , the possibility of nonlinear modal interactions increases, so more intense modal interactions for this increased initial angle of inclination of the boundary attachment are expected to be observed. Figure 13 shows the second modal response. Figure 13a and b shows the presence of a low frequency component that is deduced from the low frequency modulation of the modal response in the time domain. This is verified by the corresponding wavelet transform spectra depicted in Fig. 13c and d. One noticeable difference between the response of this nonlinear mode and its counterpart for the previous case of $\phi_0 = 0^{\circ}$ is the significant presence of the high frequency harmonics of the first nonlinear mode in the response of the second mode for the case. Additionally, a contribution from the third nonlinear mode in the response of the second mode in the experimental measurements is observed, unlike in the computational model (cf. Figure 13c and d). The conjecture is that this is due to unmodeled dynamics that are excited by nonlinear effects that are not fully captured by the FE model and the nonlinear boundary attachment, e.g., friction or unmodeled nonlinear stiffness effects.

Figure 14 depicts the response of the third nonlinear mode. Similar to the response of the second mode presented in Fig. 13, the response of the third mode contains traces of the first mode and its harmonics; however, these harmonics are not as intense and dominant as in the response of the second mode. This indicates that although the nonlinearity of the boundary attachment affects the response of the third



Fig. 12 Response of the first nonlinear mode for high impulse excitation and $\phi_0 = 16^{\circ}$ (cf. Fig. 7): a, c Computational prediction, and b, d experimental measurement

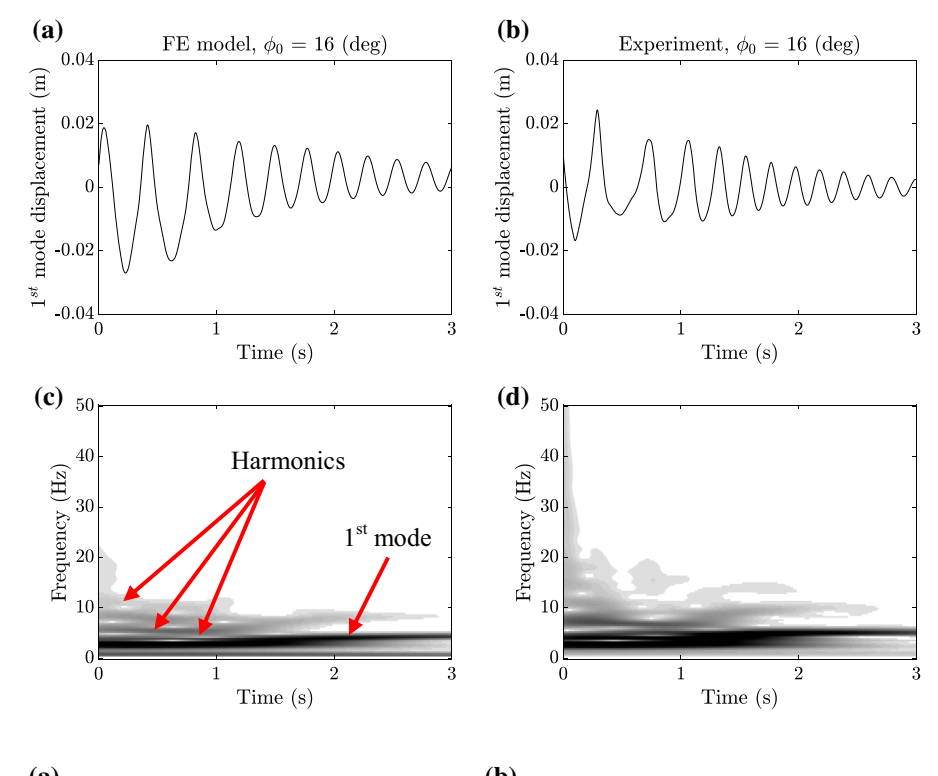
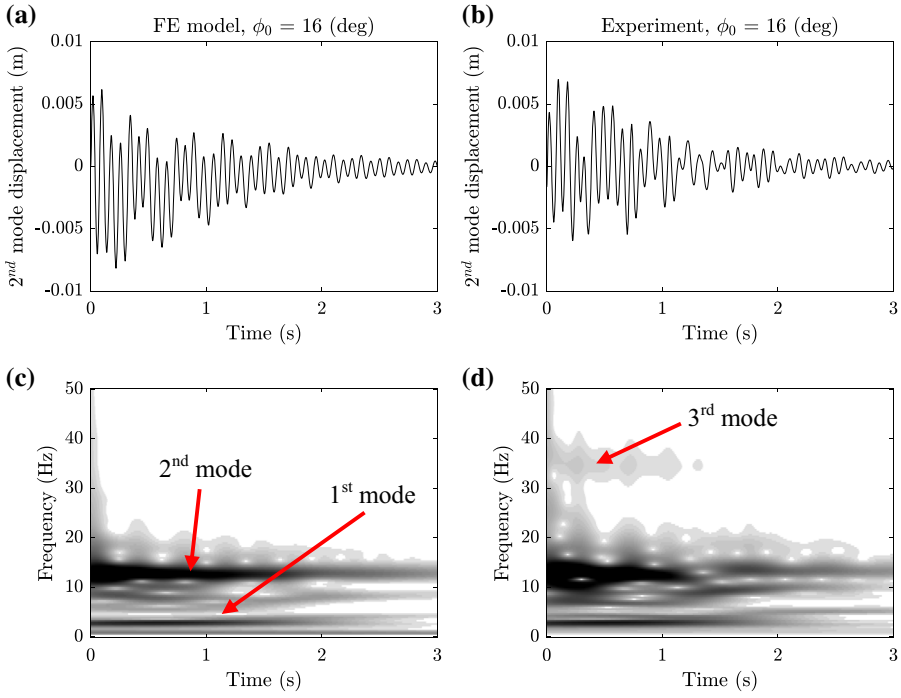


Fig. 13 Response of the second nonlinear mode for high impulse excitation and $\phi_0 = 16^{\circ}$ (cf. Fig. 7): **a**, **c** Computational prediction, and **b**, **d** experimental measurement



nonlinear mode, it is not as significant as for the first and second modes.

Similar to the previous case, the normalized instantaneous averaged modal energies and

normalized effective damping ratios for the responses of the system obtained by the computational model and the experimental measurements are computed here. Figure 15 illustrates the normalized modal



Fig. 14 Response of the third nonlinear mode for high impulse excitation and $\phi_0 = 16^{\circ}$ (cf. Fig. 7): a, c Computational prediction, and b, d experimental measurement. (Color figure online)

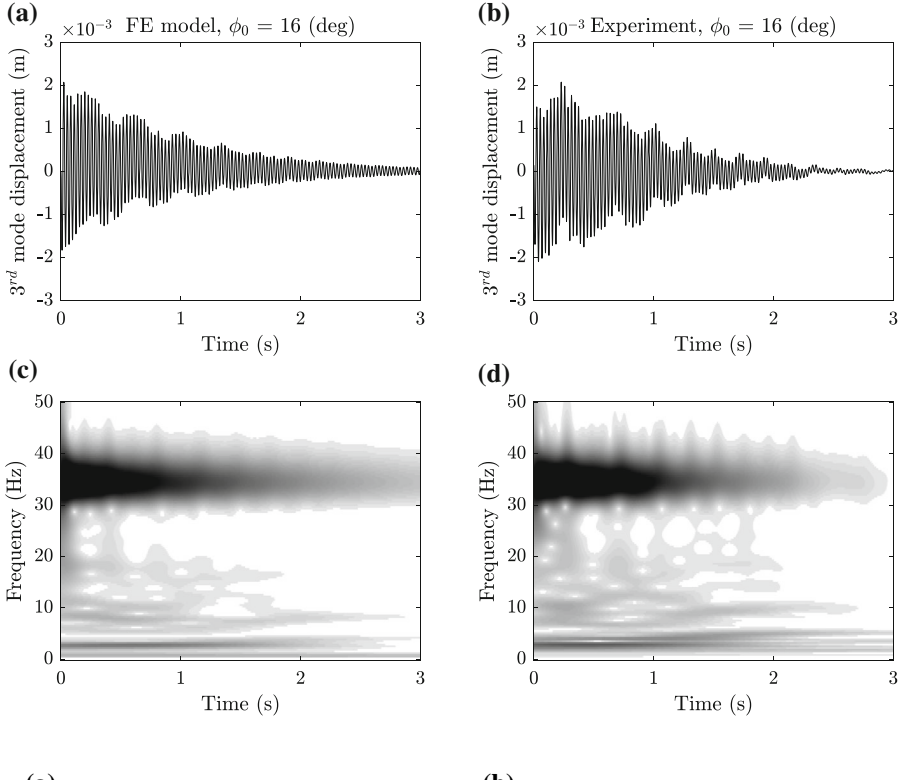
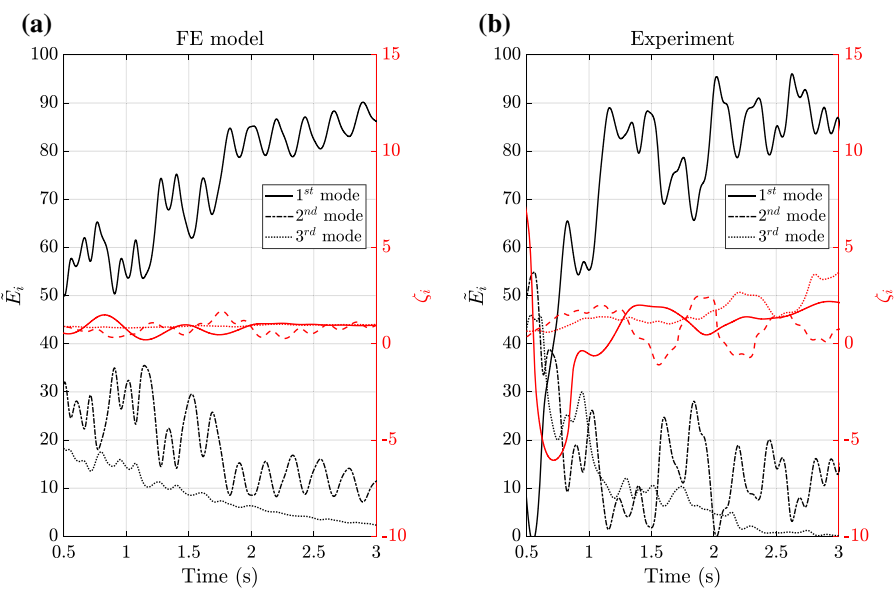


Fig. 15 Case of high impulse excitation and $\phi_0=16^\circ$ (cf. Fig. 7): Instantaneous normalized modal energies (10) (black curves–left axes) and instantaneous normalized damping ratios (12) (red curves–right axes) for the three leading cantilever modes, a Computational predictions and b experimental measurements



energies and damping ratios computed for both the response of the FE model and measured response from the experiment. Beginning with the normalized averaged modal energies—cf. black curves in Fig. 15a and b—we observe intense modal energy exchanges, especially between the first and the second nonlinear

modes of the cantilever beam. This is inferred by the high amplitude fluctuations noted in the plots, especially during the early time, highly energetic regime of the transient dynamics. Specifically, this is confirmed by the out-of-phase fluctuations of the first and second normalized modal damping ratios in both plots; being



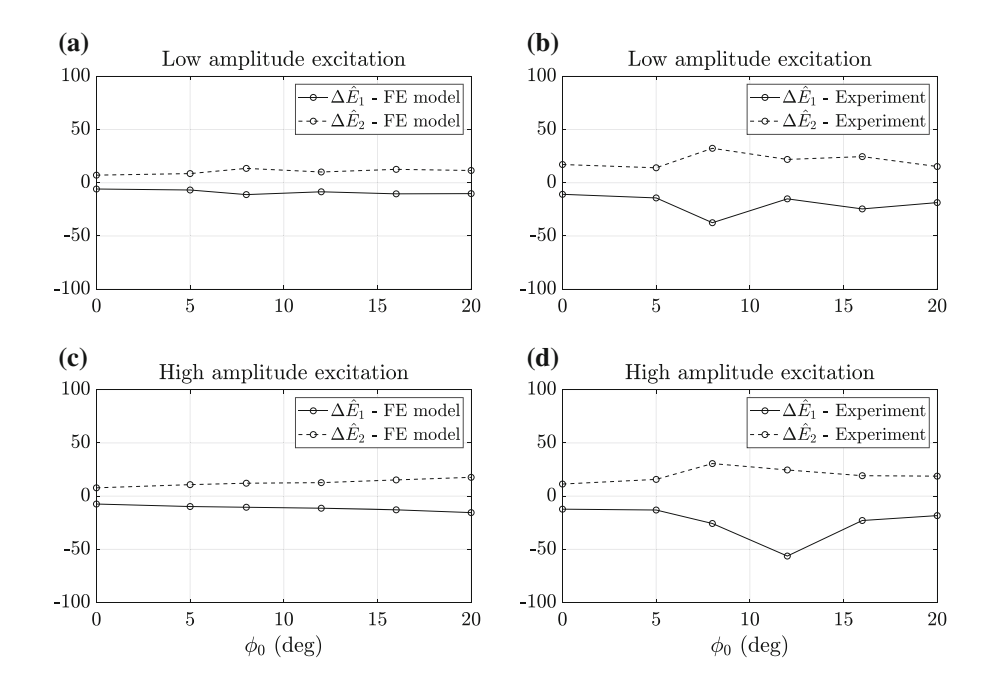
approximately of the same order of magnitude, these out-of-phase fluctuations prove that a synchronization is realized, in the sense that, as the first mode loses energy, the second mode absorbs it and then releases it back to the first mode in an recurrent fashion. Computing the scalar energy exchange measure introduced earlier, for this particular case one can determine $\Delta \hat{E}_1 = 15.24\%$ and $\Delta \hat{E}_2 = -12.85\%$ when computed from the FE model and $\Delta \hat{E}_1 = -22.88\%$ and $\Delta \hat{E}_2 = 19.21\%$ when computed from the experimental measurements.

To study the effects of the geometry of the boundary attachment, i.e., of the initial angle of inclination ϕ_0 , on the intensity of the nonlinear modal energy exchanges, the computational and experimental energy measures $\Delta\hat{E}_1$ and $\Delta\hat{E}_2$ for low (\sim 130N) and high (\sim 230N) impulsive excitations applied to the beam tip for $\phi_0=0^\circ,5^\circ,8^\circ,12^\circ,16^\circ$ and 20° are computed. The plots in Fig. 16 depict these energy measures for both low and high intensity excitations.

Starting with Fig. 16a and b, similar trends in the variations in $\Delta \hat{E_i}$, i=1,2, with ϕ_0 for the computational and experimental results are observed. Although the plots in Fig. 16a are not similar to those in Fig. 16b, both cases indicate that for weak impulsive excitations the optimum initial angle of inclination of the nonlinear attachment that maximizes the modal

energy exchanges is approximately $\phi_0=8^\circ$. Knowing that, by increasing ϕ_0 , in effect the linearity of the geometrically nonlinear boundary condition [12, 22, 24] is enhanced (in the sense that the linear part of the nonlinear stiffness characteristic increases), it is very interesting to note that the effective nonlinearity in the system is enhanced only until the angle approaches the value $\phi_0=8^{^\circ}.$ However, for strong impulse excitation the optimal value of ϕ_0 at which the modal energy exchange is maximized changes as well. The computational plots in Fig. 16c show that the optimal value of ϕ_0 in that case is greater than 20°. The experimental plots in Fig. 16d on the other hand suggest that the optimal value of the angle is approximately 12°. The discrepancy that is observed between the computational model and the experimental measurement for the case of strong impulse excitation may be caused by the effects of unmodeled stiffness and damping nonlinearities that are present in the transient dynamics of the experimental fixture, e.g., friction effects or clearance nonlinearities. In a more general context, however, the importance of the results of Fig. 16 is that it shows that the extra tunability to the system dynamics that is realized through the inclination of the nonlinear attachment enables the maximization of the nonlinear modal energy exchanges in the (otherwise linear) cantilever beam, which results in faster overall energy

Fig. 16 Maximum modal energy exchange measures, $\Delta \hat{E_i}$, i=1,2, for weak impulsive excitations as functions of ϕ_0 computed from, **a** the FE model, and **b** the experimental measurements; corresponding energy measures for strong impulsive excitations computed from **c** the FE model and, **d** the experimental measurements





dissipation in the system. This enhanced dissipative capacity is related to the nonlinear scattering of impulsive energy in the frequency domain as energy is continuously exchanged between lower frequency and higher frequency cantilever modes.

5 Concluding remarks

The modal interactions in a cantilever beam whose free end was grounded by a geometrically nonlinear element consisting of an inclined linear spring—damper pair at an initial angle ϕ_0 relative to the neutral axis of the beam were investigated. A finite element (FE) model with a geometrically nonlinear attachment was constructed to predict the measured responses of an experimental fixture. The parameters of the integrated model were estimated through a multi-step nonlinear system identification technique, incorporating a Multi-input Multi-output Frequency Domain Identification (MFDID) technique in the frequency domain, and time series reconciliation.

Using the identified computational model, a theoretical framework was developed to study the modal responses of the beam by projecting its responses on the linearized modal basis obtained at the low energy limit of the transient dynamics. As a first step, the modal responses of the system for two different magnitudes of impulsive excitation and different initial angles of inclination ϕ_0 were computed and studied. The following observations can be made.

In all cases examined, a prominent presence of the first nonlinear mode of the beam in the wavelet transform spectrum of the response of the second nonlinear mode was observed. To verify this observation, the time-averaged modal energies and instantaneous damping ratios of the nonlinear modes of the beam were computed, and intense modal energy exchanges, especially between the first and second modes, were observed.

After estimating the time-averaged modal energies of the system, the maximum amount of energy exchanged between the first and second modes for varying impulse intensity and angles of inclination ϕ_0 was computed. In the case of low intensity impulses, both the experimental and computational results confirmed that there exists an optimal initial angle of inclination, $\phi_0 \approx 8^\circ$, where the nonlinear modal

energy exchanges reach their maximum values. For high intensity impulsive excitations, on the other hand, the computational model predicted an optimal angle greater than $\phi_0=20^{\circ}$, while the results obtained from the experimental measurements indicated that the maximum modal energy exchange occurred at an angle of $\phi_0\approx 12^{\circ}$. It was conjectured that unmodeled dynamics was the reason for this discrepancy, the effects of which are enhanced as the intensity of the impulsive excitation increases.

Fluctuations in the maximum modal energy exchanges between the first and second beam modes for both low and high intensity impulsive excitations confirmed that one can induce modal energy exchanges in the cantilever beam by introducing geometric nonlinearity at its boundary. The propensity of the governing nonlinear modes of the system to exchange energy can be increased significantly with increasing energy and varying angle of inclination of the boundary attachment, thereby increasing the overall dissipative capacity of the system through frequency scattering of energy in the frequency domain.

The studied nonlinear mechanism of energy scattering in the frequency domain, i.e., the modal space of the primary structure, enhances the dissipative capacity of the cantilever beam, without the need to add any mass or damping. In fact, the enhanced dissipative capacity of the beam with the nonlinear boundary condition is due to better utilization of the inherent dissipative capacity of the beam itself, through low-to-high energy transfers and excitation of higher-order beam modes. This approach can provide an alternative way for efficient and rapid energy dissipation in flexible structures, compared to current methods based, e.g., on the use of dynamic absorbers or additional damping devices.

Funding This work was supported in part by NSF Grant No. CMMI-17-1727761 and by the China Scholarship Council and the Jiangsu Innovation Program for Graduate Education (YL) under Grant No. KYCX17-0233 (Fundamental Research Funds for Central Universities).

Compliance with ethical standards

Conflict of interest The authors declare that they have no conflict of interest.



References

- AL-Shudeifat, M.A.: Highly efficient nonlinear energy sink. Nonlinear Dyn. 76, 1905–1920 (2014)
- AL-Shudeifat, M.A., Saeed, A.S.: Frequency-Energy Dependence of the Bistable Nonlinear Energy Sink, In ASME 2017 International Design Engineering Technical Conferences and Computers and Information in Engineering Conference (2017)
- AL-Shudeifat, M.A., Vakakis, A.F., Bergman, L.A.: Shock mitigation by means of low-to high-frequency nonlinear targeted energy transfers in a large-scale structure. J. Comput. Nonlinear Dyn. 11, 021006 (2015)
- Gendelman, O.V., Vakakis, A.F.: Introduction to a topical issue 'nonlinear energy transfer in dynamical and acoustical systems', philosophical transactions of the royal society a: mathematical. Phys. Eng. Sci. 376, 20170129 (2018)
- Gourdon, E., Alexander, N.A., Taylor, C.A., Lamarque, C.H., Pernot, S.: Nonlinear energy pumping under transient forcing with strongly nonlinear coupling: theoretical and experimental results. J. Sound Vib. 300, 522–551 (2007)
- Habib, G., Romeo, F.: The tuned bistable nonlinear energy Sink. Nonlinear Dyn. 89, 179–196 (2017)
- Hubbard, S.A., McFarland, D.M., Bergman, L.A., Vakakis, A.F.: Targeted energy transfer between a model flexible wing and nonlinear energy sink. J. Aircraft 47, 1918–1931 (2010)
- Hubbard, S.A., McFarland, D.M., Bergman, L.A., Vakakis, A.F., Andersen, G.: Targeted energy transfer between a swept wing and winglet-housed nonlinear energy Sink. AIAA J. 52, 2633–2651 (2014)
- Ji, J.C.: Application of a weakly nonlinear absorber to suppress the resonant vibrations of a forced nonlinear oscillator. J. Vib. Acoust. 134, 044501 (2012)
- Lee, Y.S., Nucera, F., Vakakis, A.F., McFarland, D.M., Bergman, L.A.: Periodic orbits, damped transitions and targeted energy transfers in oscillators with vibro-impact attachments. Physica D 238, 1868–1896 (2009)
- Li, T., Lamarque, C.-H., Seguy, S., Berlioz, A.: Chaotic characteristic of a linear oscillator coupled with vibro-impact nonlinear energy sink. Nonlinear Dyn. 91, 2319–2330 (2018)
- Liu, Y., Mojahed, A., Bergman, L.A., Vakakis, A.F.: A new way to introduce geometrically nonlinear stiffness and damping with an application to vibration suppression. Nonlinear Dyn. 96, 1819–1845 (2019)
- Manevitch, L.I., Sigalov, G., Romeo, F., Bergman, L.A., Vakakis, A.: Dynamics of a linear oscillator coupled to a bistable light attachment: analytical study. J. Appl. Mech. 81, 041011 (2013)
- McFarland, D.M., Bergman, L.A., Vakakis, A.F.: Experimental study of non-linear energy pumping occurring at a single fast frequency. Int. J. Non-Linear Mech. 40, 891–899 (2005)
- Moore, K.J., Mojahed, A., Bergman, L.A., Vakakis, A.F.: Local nonlinear stores induce global dynamical effects in an experimental model plane. AIAA J. 57, 4953–4965 (2019)
- Pennisi, G., Mann, B.P., Naclerio, N., Stephan, C., Michon, G.: Design and experimental study of a nonlinear energy sink coupled to an electromagnetic energy Harvester. J. Sound Vib. 437, 340–357 (2018)

- Qiu, D., Li, T., Seguy, S., Paredes, M.: Efficient targeted energy transfer of bistable nonlinear energy sink: application to optimal design. Nonlinear Dyn. 92, 443–461 (2018)
- Saeed, A.S., AL-Shudeifat, M.A., Vakakis, A.F.: Rotary-oscillatory nonlinear energy sink of robust performance. Int. J. Non-Linear Mech. 117, 103249 (2019)
- Vakakis, A., Gendelman, O., Manevitch, L., McCloskey, R.: Energy pumping in nonlinear mechanical oscillators I: dynamics of the underlying hamiltonian system. J. Appl. Mech. Trans. ASME 68, 34–41 (2001)
- Vakakis, A.F., Gendelman, O.V., Bergman, L.A., McFarland, D.M., Kerschen, G., Lee, Y.S.: Nonlinear Targeted Energy Transfer in Mechanical and Structural Systems. Springer, Berlin (2008)
- Carrella, A., Brennan, M.J., Waters, T.P.: Static analysis of a passive vibration isolator with quasi-zero-stiffness characteristic. J. Sound Vib. 301, 678–689 (2007)
- Mojahed, A., Moore, K., Bergman, L.A., Vakakis, A.F.: Strong geometric softening-hardening nonlinearities in an oscillator composed of linear stiffness and damping elements. Int. J. Non-Linear Mech. 107, 94–111 (2018)
- Sarlis, A.A., Pasala, D.T.R., Constantinou, M.C., Reinhorn, A.M., Nagarajaiah, S., Taylor, D.P.: Negative stiffness device for seismic protection of structures. J. Struct. Eng. 139, 1124–1133 (2013)
- Mojahed, A., Bergman, L.A., Vakakis, A.F.: Tunable-withenergy intense modal interactions induced by geometric nonlinearity. Part C J. Mech. Eng. Sci. (2020). https://doi. org/10.1177/0954406220908621
- Andersen, D., Starosvetsky, Y., Vakakis, A., Bergman, L.: Dynamic instabilities in coupled oscillators induced by geometrically nonlinear damping. Nonlinear Dyn. 67, 807–827 (2012)
- Amabili, M.: Nonlinear damping in large-amplitude vibrations: modelling and experiments. Nonlinear Dyn. 93, 5–18 (2018)
- Amabili, M.: Derivation of nonlinear damping from viscoelasticity in case of nonlinear vibrations. Nonlinear Dyn. 97, 1785–1797 (2019)
- Amabili, M.: Nonlinear damping in nonlinear vibrations of rectangular plates: derivation from viscoelasticity and experimental validation. J. Mech. Phys. Solids 118, 275–292 (2018)
- Kim, S.B., Spencer, B.F., Yun, C.-B.: Frequency domain identification of multi-input, multi-output systems considering physical relationships between measured variables. J. Eng. Mech. 131, 461–472 (2005)
- Guyan, R.J.: Reduction of stiffness and mass matrices. AIAA J. 3, 380-380 (1965)
- Moore, K.J., Kurt, M., Eriten, M., McFarland, D.M., Bergman, L.A., Vakakis, A.F.: Wavelet-bounded empirical mode decomposition for measured time series analysis. Mech. Syst. Signal Process. 99, 14–29 (2018)
- Sapsis, T.P., Dane Quinn, D., Vakakis, A.F., Bergman, L.A.: Effective stiffening and damping enhancement of structures with strongly nonlinear local attachments. J. Vib. Acoust. 134, 011016 (2012)

Publisher's Note Springer Nature remains neutral with regard to jurisdictional claims in published maps and institutional affiliations.

